8th World Conference on Experimental Heat Transfer, Fluid Mechanics, and Thermodynamics
June 16-20, 2013, Lisbon, Portugal

HEAT TRANSFER AND FLOW CHARACTERISTICS OF A PAIR OF ADJACENT SYNTHETIC JETS

Eoin Fanning, Tim Persoons and Darina B. Murray

Department of Mechanical and Manufacturing Engineering, Trinity College, Dublin 2, Ireland
E-mail : efanning@tcd.ie

ABSTRACT

The local convective heat transfer rates to an impinging synthetic jet has been shown to rival that of a steady impinging jet. A single synthetic jet still requires an external cross flow to avoid recirculation of heated fluid. However, this requirement can be avoided by operating multiple adjacent synthetic jets in an impingement setup. This paper presents the findings of an experimental study to optimize the orifice-to-impingement distance *H* and orifice-to-orifice separation distance *S*. The convective heat transfer coefficient is determined on an electrically heated metal foil using thermal imaging. The jets are driven by a pair of adjacent jet actuators forcing air through two rectangular slot orifices of width D = 1.65mm and aspect ratio α = 27:1. The jets are maintained at a constant Reynolds number and stroke length ($Re \cong 265$, $L_0/D = 29$). For the parameter range considered, an optimum setting of H/D = 24 and S/D = 3 operated within a phase difference region of $60° < \Phi < 120°$ gives the best cooling performance. The thermal imaging measurements at these settings are supplemented with particle image velocimetry (PIV) measurements of the flow field between the jet orifices and the impingement surface.

Keywords : *Synthetic Jet, Impinging Jet, vortex pair, vectoring, cross-flow, electronics cooling, particle image velocimetry*

1. INTRODUCTION

Impinging synthetic jets have been identified as a promising alternative to conventional steady cooling jets [1–3]. The primary advantage is that synthetic jets recycle ambient fluid and hence have a zero net mass-flux (ZNMF). As a result, there is no need for an external pressurized supply of fluid.

The flow structure of a synthetic jet comprises of a train of vortices. This train of vortices is formed by repeated suction and ejection of ambient fluid into and out of a cavity via an orifice driven by an oscillating diaphragm or membrane. For an orifice width D the Reynolds number $Re = \rho U_0 D/\mu$ and dimensionless stroke length L_0/D govern the flow field of a free synthetic jet.

The flow structure of an impinging synthetic jet is further characterized by the orifice-to-impingement surface distance H which determines the propagation distance of the vortices and the level of confinement and recirculation. It has been suggested [4,5] that for impingement cooling there is an optimal H/D value where a balance between vortex mixing and turbulent mixing and a sufficiently wide impingement area is observed. The distance travelled by the vortex pair not only depends on H but on the amount of fluid ejected per stroke i.e. the stroke length L_0 [1,5,6]. Valiorgue et al. [7] related both orifice-to-impingement distance and stroke length and found a critical $L_0/H \cong 2.5$. For values below this, the heat transfer rates are significantly affected by stroke length and for values above, they are independent of stroke length. Extending these findings to a wider range of stroke lengths and orifice-to-surface distances, Persoons et al. [8] developed a correlation for the stagnation Nusselt number for a single axisymmetric impinging synthetic jet. The results demonstrated a convective heat transfer rate similar to that of a steady impinging jet.

The key advantage of operating synthetic jets side-by-side is that a phase difference Φ between the jets can induce a cross-flow which draws fresh cooling fluid to the jet eliminating the need for an external cross-flow (e.g. driven by a fan). This was demonstrated by Persoons et al. [9] using particle image velocimetry (PIV) to measure velocity in the flow field of a pair of synthetic jets impinging on a heated foil. It was demonstrated that the vectoring of the jet caused by phase difference [10,11] sets up a cross flow which draws fresh cooling fluid to the jet.

Combining the PIV measurements with thermal imaging of the heated foil, Persoons et al. [9] determined an optimum phase difference region of $90° < \Phi < 120°$ for constant values of Re = 300, L_0/D = 29 and an orifice centre-to-centre separation $S = 3D$. In this range of phase difference an effective cross-flow was set up whilst maintaining strong vortex mixing, resulting in the highest convective heat transfer rates.

The current work extends these PIV and thermal imaging measurements to a wider range of geometric parameters, including the orifice-to-impingement surface distance H and the orifice centre-to-centre distance S.

2. EXPERIMENTAL METHOD

2.1 Impinging Synthetic Jet Test Setup

Figure 1 illustrates the main components of the test setup. Two speakers inside rectangular cavities force ambient air through an accurately-machined plastic orifice plate 10 mm in thickness with a slot width of D = 1.65 mm and length 44.5 mm (aspect ratio = 27:1). The values of H and S were adjusted using machined acrylic spacers.

A relationship between the jet velocity amplitude U_m* and cavity pressure amplitude p* [12] is shown below:

$$\frac{\rho a U_m^*}{p^*} = \left(\frac{2V_c}{AL'}\right)^{\frac{1}{2}} \times \left(\left(\frac{f}{f_0}\right)^2 + \left[\left(\frac{f}{f_0}\right)^4 + \left(\frac{KV_C}{A'^{L'}}\frac{p\,*}{\rho a^2}\right)^2\right]^{\frac{1}{2}}\right)^{-\frac{1}{2}} \quad (1)$$

L' is the effective orifice length, a is the speed of sound, f_0 is the Helmholtz resonance frequency ($= a/(2\pi L')[A'L'/V_C]^{1/2}$), V_C

is the cavity volume and *A'* is the orifice cross sectional area. This was used in order to estimate the time-averaged jet velocity $\underline{U}_0 = U_m^*/\pi$ for sine wave excitation. Hence *Re* and L_0 ($L_0 = \int_{t=0}^{1/(2f)} U_m dt = U_0/f$) are calculated from U_0. Using a high pressure microphone to record cavity pressure, *Re* and L_0 could be maintained at a fixed value.

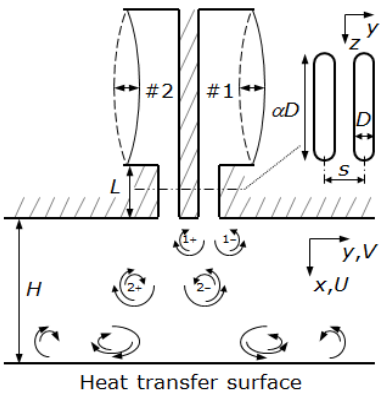

Figure 1 – Impinging synthetic jet test facility

2.2 Convective Heat Transfer Coefficient

An electrically heated constantan foil (0.15m x 0.145m) was used as the impingement surface. The foil is sufficiently thin (10 µm) to be considered a constant heat flux boundary. The underside of the foil was sprayed with a high emissivity matte black paint and hence a thermal imaging camera (FLIR Systems Thermovision A40M) was used to measure the distribution of temperature across the foil. K type thermocouples were used to record air temperatures at different points in the test section. The convective heat flux q'' [W/m^2] is determined from the electrical power to the foil q''_{ohm} and corrected for heat losses due to: radiation q''_{rad} from the foil surfaces (top and bottom); natural convection q''_{cnv} from the bottom of the foil and; spreading of heat across the foil from lateral conduction q''_{cnd}; such that:

$$q'' = q''_{ohm} - q''_{rad} - q''_{cnv,bot} + q''_{cnd} = h(T - T_{jet}) \quad (2)$$

T and T_{jet} are the local foil temperature and jet cavity air temperature measured with uncertainties of approximately 0.05°*C* and 0.1°C, respectively. The maximum uncertainty of the heat transfer coefficient *h* values ranged from 7 - 9%.

2.3 Flow Field

The PIV system currently being used to perform velocity field measurements consists of a New Wave Solo-II Nd:YAG twin cavity laser (30mJ, 15Hz) and a PCO Sensicam™ thermo-electrically cooled CCD-camera (1280×1024 px^2, 12 bit) with 28 mm lens. A 0.3mm thick laser sheet is generated using a collection of laser optics and the flow is seeded with a LaVision Aerosol Generator. The seeding fluid is Di-Ethyl-Hexyl-Sebacat ($C_{26}H_{50}O_4$), 0.2 – 0.3 µm in diameter.

The CCD camera, mounted perpendicular to the laser sheet and phase-locked to the synthetic jet speaker, captures images for 24 phases per cycle. Vector fields are averaged for each phase. The velocity fields are processed using LaVision DaVis 7.2 software, using a multipass algorithm with continuous window deformation (initial interrogation window size 64 × 64 px^2 and 50% window overlap, final interrogation window size 32 × 32 px^2 and 75% window overlap using Whittaker reconstruction in the final pass). Four vector fields are averaged for each phase.

3. RESULTS AND DISCUSSION

Flow and convective heat transfer measurements of the synthetic jet pair have been carried out for the following geometric settings: (a) Orifice-to-impingement distance of H = 24D, 12D and 6D (for S = 3D); (b) Orifice-to-orifice distance of S/D = 3, 4.5, 6, and 12 (for H/D = 12). All experiments were carried out for a constant stroke length of L_0/D = 29. Note that while all heat transfer measurements were performed at a Reynolds number of *Re* = 300, the PIV measurements were performed at *Re* ≅ 265.

3.1 Flow characteristics

Figure 2 shows the flow measurement results for the different values of *H* and *S*. The results are plotted as time-averaged streamlines and velocity magnitude $|UV|^*$ normalized with the characteristic velocity U_0, such that $|UV|^* = (U^2+V^2)^{1/2}/U_0$.

3.1.1 Effect of orifice-to-impingement distance

Figures 2a-d show that quite distinct flow fields exist for the smallest and largest orifice-to-impingement distances (H=6D and H=24D, respectively). For a jet pair in phase (a) at H = 6D the jets are separately impinging the surface whereas for the H = 24D a single wider fully merged jet is observed. Figure 3 shows vorticity plots and vector fields which are phase-locked roughly at the point of impingement for the different H/D values (at Φ = 0°). Figure 3c demonstrates an enhanced or merged vortex pair when operated in phase for H = 24D similar to a free synthetic jet pair [10,11]. The available propagation distance between the orifice plate and the impingement surface is too small for an enhanced vortex pair to establish for H = 6D as shown in figure 3a.

The intermediate setting of H = 12D (figure 3b) does not demonstrate the wide jet profile that is seen for H = 24D, when operated in phase. It does, however, demonstrate merging of adjacent vortex pairs into an enhanced vortex pair just as they reach the impingement surface, forming a semi-merged jet. For a lower H/D value, the vorticity appears to significantly increase but the width of the jet centre velocity field reduces. This suggests a trade-off between vortex strength at impingement and the size of the impingement zone of the jet.

Figures 2b and 2d demonstrate the effect of increasing the phase difference to Φ = 135° for H = 6D and 24D, respectively. For H = 24D we see a vectoring effect as seen for an impinging jet pair in previous work by Persoons et al. [9] towards the jet

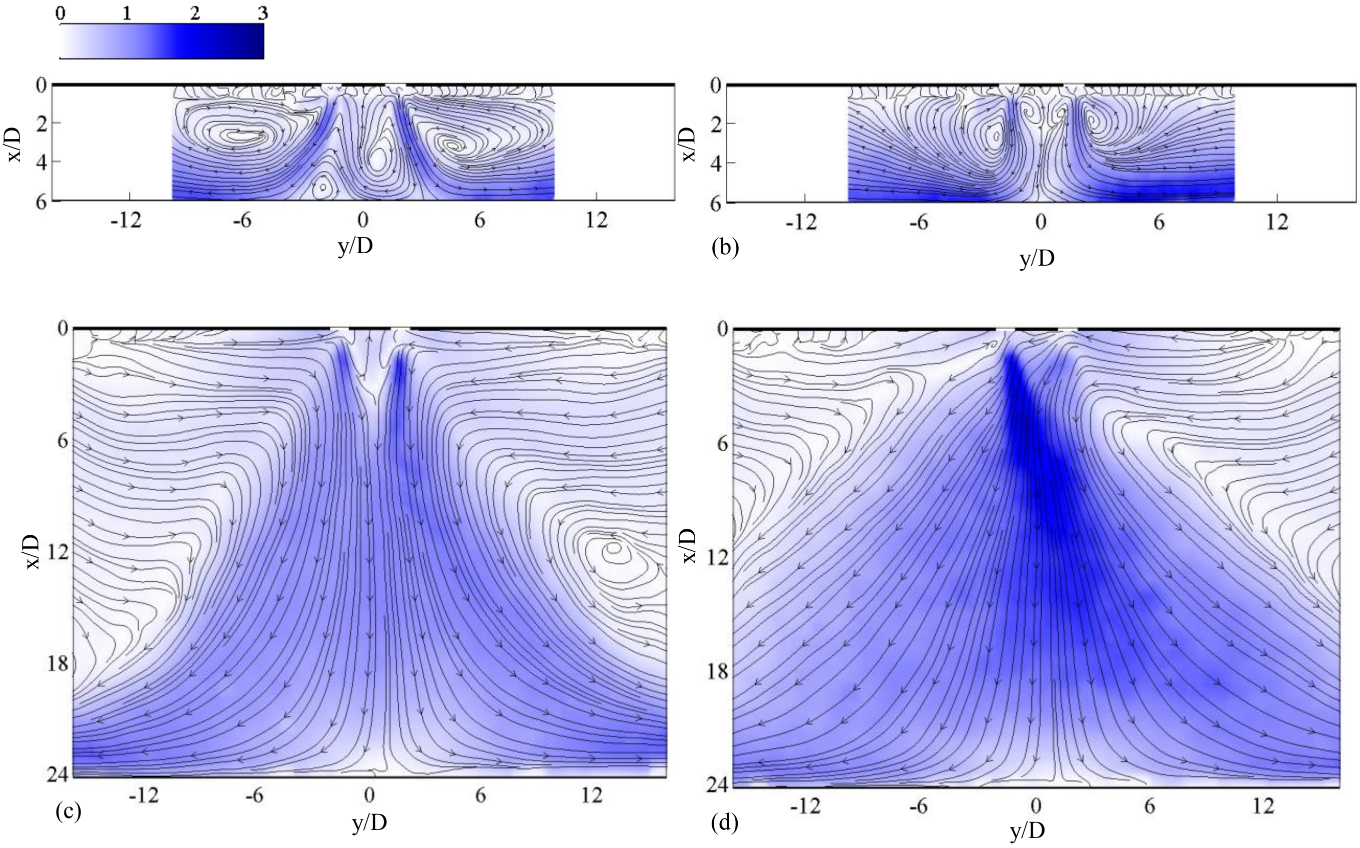

Figure 2 – Time-averaged streamlines and velocity magnitude $(U^2+V^2)^{1/2}/U_0$ plot of impinging synthetic jet pair flow field at L_0 = 29*D* and *Re* ≅ 265 (a,b) Φ = 0° and 135° for *H* = 6*D, S* = 3*D*; (c,d) Φ = 0° and 135° for *H* = 24*D, S* = 3*D*;

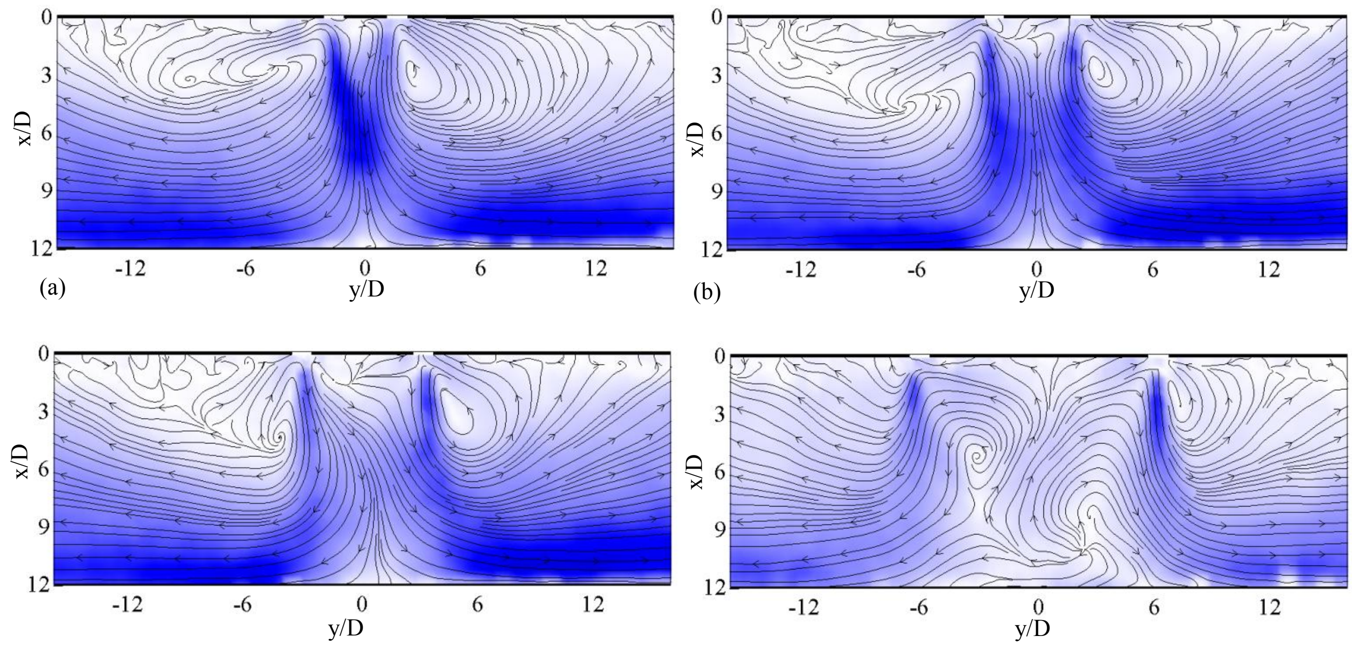

Figure 3 - Time-averaged streamlines and velocity magnitude $(U^2+V^2)^{1/2}/U_0$ plot of impinging synthetic jet pair flow field at L_0 = 29*D*, *Re* ≅ 265, *H* = 12*D* and Φ = 135° for (a) *S* = 3*D*, (b) *S* = 4.5*D*, (c) *S* = 6*D* and (d) *S* = 12*D*

leading in phase (right). For the smaller distance of $H = 6D$ the jets are attracted towards each other. This results in a more narrow time-averaged jet profile as seen in figure 2b. Vorticity measurements and plots at this phase difference have illustrated a train of vortex pairs from either orifice impinging on the surface centre ($x/D = y/D = 0$). This is shown by the single stagnation point in figure 2b compared to the double stagnation points in figure 2a.

Another interesting feature of the small orifice-to-impingement distance $H = 6D$ is the much more pronounced recirculation region on the outer side of each orifice for two in-phase jets (figure 2a) compared to the jets when they are driven at a phase difference of $\Phi = 135°$ (figure 2b). This is due to out-of-phase impinging vortex pairs being affected by the suction stroke of their opposite orifice as they try to migrate outward from the impingement zone. While this does not happen for in-phase vortex pairs, their inner vortices however, do not travel away from the impingement zone at all since they are attracted to each other and become 'trapped' in the centre. This is shown by the two recirculation regions between the jets in figure 2a.

This effect is less pronounced as H/D is increased since directly after impingement, the vortex pairs have propogated further away from the orifice and are thus less affected by suction from the opposite orifice.

Figure 2e shows the flow field for the intermediate orifice-to-impingement distance $H = 12D$ at a phase difference of $\Phi = 135°$. As is the case for $H = 6D$, we see an attraction of the jets towards each other when driven out of phase and hence a train of vortex pairs impinging the centre of the impingement surface.

3.1.2 Effect of orifice-to-orifice distance

Figures 3a-d illustrate the effect of the orifice-to-orifice distance S on the mean flow field. As the separation distance is increased, a reduction in the attraction of the jets towards their opposite orifice is observed. This can be seen in the direction of the streamlines normal to the orifice plane. As S/D is increased for a phase difference of $\Phi = 135°$, the angle of the jets to the orifice plane approaches a right angle. For $S = 3D$, $4.5D$ and $6D$ (figure 3a-c), the streamlines demonstrate a train of vortex pairs impinging on the impingement surface centre as seen for the smaller H/D value of 6 when driven out of phase.

For the largest orifice-to-orifice distance of $S = 12D$ (Figure 3d), the jets impinge either side of the foil centre, demonstrating little or no attraction towards their opposite orifice. In the region between the jet orifices, two counter-rotating circulation regions can be observed here. This is because the distance between the orifices is too large for the inner vortices to travel outward from the impingement zone sufficiently before the opposite jet is ejected. As a result, the inner vortex becomes 'trapped' in between the orifices since it is attracted to the counter-rotating inner vortex of the opposite jet. This effect is similar to that mentioned above for an in-phase jet pair operated at the geometric settings $H = 6D$ and $S = 3D$. Both effects suggest possible critical values of H/Φ and S/Φ at which the inner vortices are not subjected to this interference.

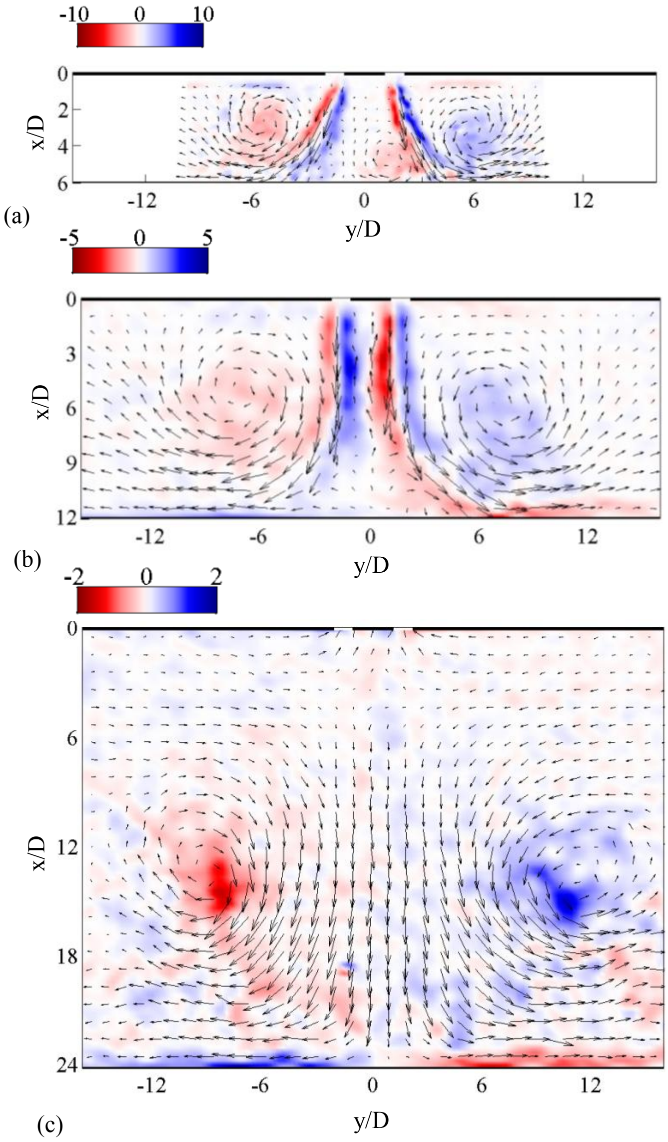

Figure 4 – Phase-locked plots of dimensionless vorticity $\omega D/U_0$ of an impinging synthetic jet pair flow field for L_0 = 29*D*, *Re* ≅ 265, Φ = 0° for *S/D* = 3 at (a) *H* = 6*D*, (b) *H* = 12*D*, and (c) *H/D* = 24

3.1.3 Cross-flow Mechanism

An important heat transfer mechanism observed in the PIV measurements by Persoons et al. [9] was a net cross flow ΔV which drew fresh cooling fluid to the jet. This net cross-flow was induced by the vectoring effect of the jet and its direction was towards the jet leading in phase. The velocity can be quantified by integrating the transverse velocity V along the channel height (orifice-to-impingement distance H), such that:

$$\Delta V = \frac{1}{H}\int_0^H V dx|_{y\to-\infty} + \frac{1}{H}\int_0^H V dx|_{y\to+\infty}$$

Persoons et al. [9] observed a monotonic increase in the magnitude of the cross-flow with phase difference between the jet pair, reaching a peak value of $\Delta V = 0.17U_0$ at $\Phi = 180°$ (for $H = 24D$, $S = 3D$, $Re = 300$ and $L_0 = 29D$). This current study did not reveal a consistent increase or trend in the net cross-flow with Φ for the same dimensionless stroke length across all values of H and S tested. However, when the phase difference was increased to $\Phi = 180°$ a particularly strong cross-flow of $\Delta V = 0.5U_0$ was observed. Since the governing parameters and settings were unchanged from the measurements of Persoons et al. [9], it is possible that the cross-flow effect is highly sensitive to the orifice edge geometry which may have changed slightly over time. This is a possible explanation for the different trends of cross-flow with Φ.

The flow field is shown in Figure 5a for this particular setting ($H = 24D$, $S = 3D$ and $\Phi = 180°$). The time-averaged streamline plot demonstrates a significant cross-flow in the direction of the jet leading in phase (right-hand side). In the formation region of the jet pair, it can be observed that the left jet is being vectored or tilted towards the right jet. The flow field in the region near the right orifice is quite similar to that of a free synthetic jet pair operated at large values of Φ as shown by Smith and Glezer [10] for the same dimensionless stroke length. Their measurements demonstrated a free jet flow that was predominantly parallel or attached to the orifice surface in the direction of the jet leading in phase.

Figures 5b and 5c illustrate how the cross-flow is no longer present as the orifice-to-impingement distance is reduced to $H = 12D$ and $6D$, respectively, for $\Phi = 180°$. The net cross-flow was calculated to be $\Delta V = 0.01U_0$ for both of these settings. There is some vectoring present and a recirculation region near the left orifice for $H = 12D$. However, the velocity magnitude and streamline direction become increasingly symmetric across the y direction as the H/D value is reduced. Thus, the close proximity of the impingement surface reduces the effect of this cross-flow and the train of vortex pairs (described in section 3.1.1) becomes the dominant heat transfer mechanism.

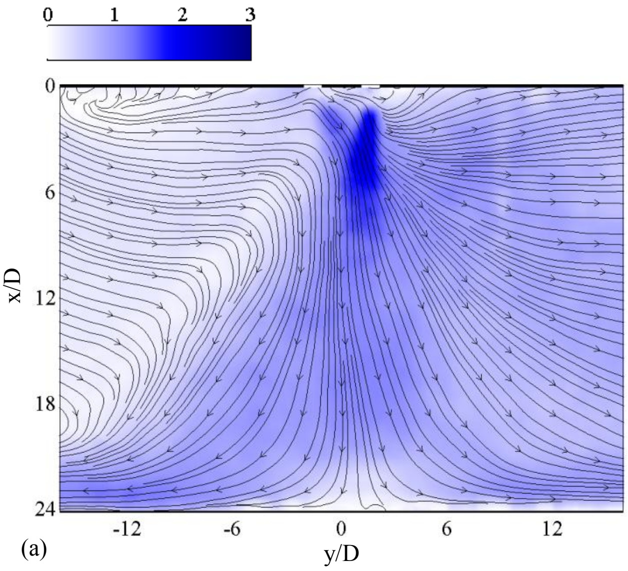

(a)

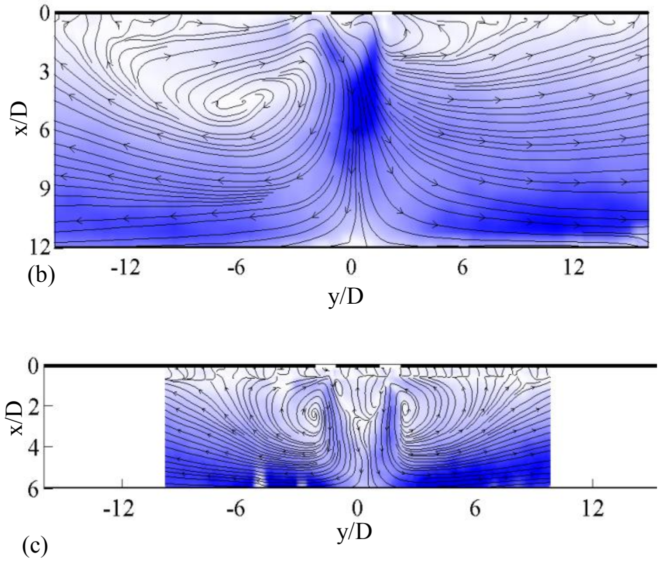

(b)

(c)

Figure 5 – Time-averaged streamlines and velocity magnitude $(U^2+V^2)^{1/2}/U_0$ plot of impinging synthetic jet pair flow field for $\Phi = 180°$ and $S = 3D$ for (a) $H = 24D$, (b) $H = 12D$ and (c) $H = 6D$;

3.2 Heat Transfer Characteristics

The local heat transfer coefficient distribution across a heated impingement foil was measured for the same geometric settings as in the PIV measurements and for each setting the phase difference was varied from $\Phi = 0°$ to $180°$ in intervals of 15°. These distributions are shown in Figure 6 for the smallest and largest distances ($H = 6D$, $24D$; $S = 3D$, $12D$) at a phase difference of $\Phi = 135°$.

Figure 7 shows the maximum local Nusselt number Nu_{max} for different orifice-to-impingement and orifice-to-orifice distances, respectively, as a function of phase difference. In summary, these results demonstrate higher maximum heat transfer rates as both the orifice-to-impingement distance and orifice-to-orifice distance are minimized. Note that the Nusselt number and Reynolds number are calculated using the characteristic slot width D as used in previous studies [8, 9] rather than the hydraulic diameter $D_h \cong 2D$.

3.2.1 Effect of orifice-to-impingement distance

By examining the jet stagnation zones in Figure 6a and b, a trade-off can be seen between local maximum heat transfer coefficients and spatial-averaged heat transfer coefficient as the H/D value is increased. These distributions supplemented with the PIV measurements above suggest this trade-off is due to a train of coherent vortex pairs impinging the foil for lower H/D values, whereas for higher H/D values a wider vectored jet is witnessed (see figure 2b and 2d).

An enhancement of stagnation heat transfer with phase difference Φ is evident in Figure 7a. Interestingly, this enhancement is even more pronounced for smaller values of H/D. This trend can be explained by the interference effect for low H/D described in Section 3.1.1. For smaller phase differences, the individual impinging vortex pairs are affected by the suction of their opposite orifice. This means the mixing mechanism of the vortices as they travel outward from the stagnation point is not as strong for low phase differences. For in-phase jets, the inner vortices of the pairs do not travel outward from the centre at all and become trapped or coalesced between the jets.

The region of optimum phase difference Φ appears to shift with H/D. The interference effect mentioned above does not affect impingement heat transfer for larger H/D values since the impingement surface is too far from the orifices. A loss in heat transfer for larger values of Φ is possibly caused by over-vectoring of the jet since the vortices travel further and hence dissipate more, as observed by Persoons et al. [9] for $H = 24D$.

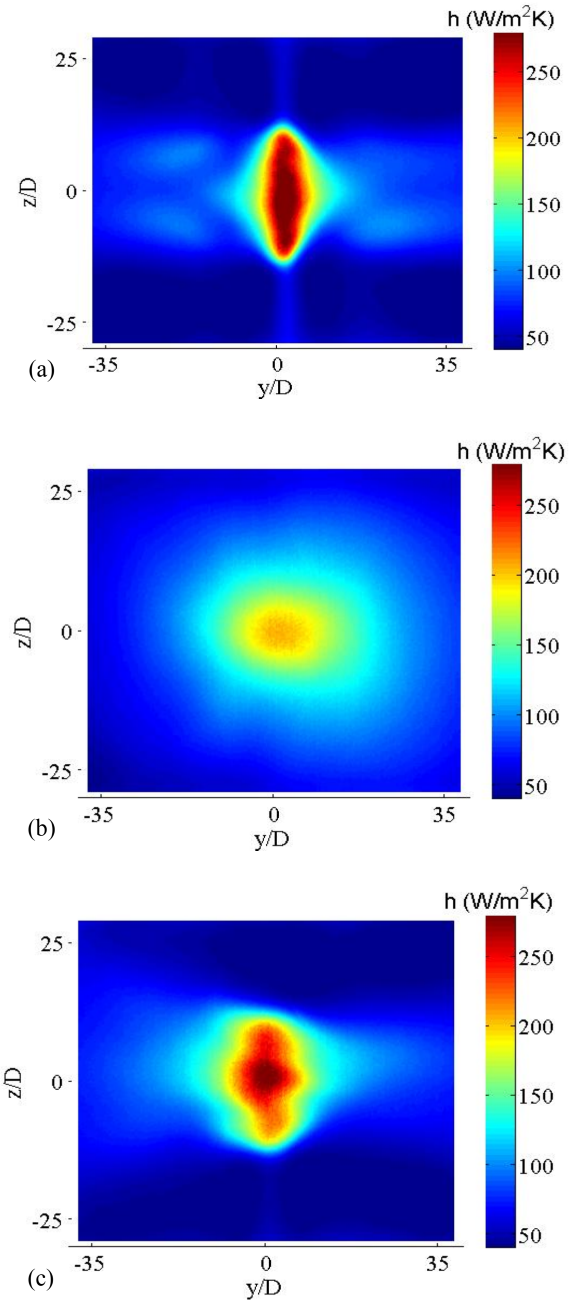

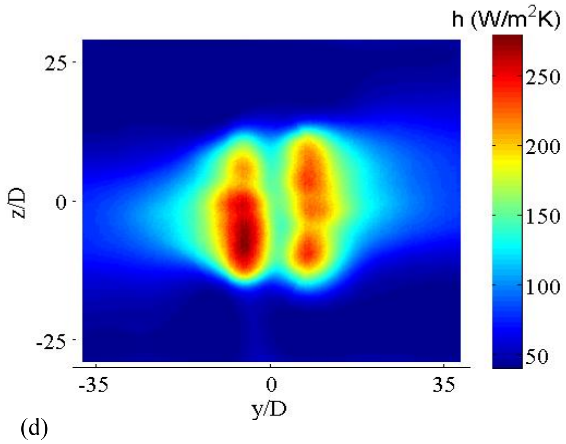

Figure 6 - Heat transfer coefficient distributions for two jets running at a phase difference of Φ = 135° for *Re* = 300, L_0/D = 29: for *S*=3*D* (a) *H*=6*D*, (b) *H*=24*D*; and for *H*=12*D* (c) *S*=3*D*, (d) *S*=12*D*;

3.2.2 Effect of orifice-to-orifice distance

As the orifice-to-orifice spacing is increased, a loss in local maximum heat transfer in the stagnation zone is exhibited. This is likely related to the loss of attraction of the jets towards their opposite orifice as explained in section 3.1.2. The twin peaks in the stagnation zone of Figure 6d suggest that the vortex pairs are impinging the foil individually rather than as a train of vortex pairs as illustrated by the single peak in Figure 6c

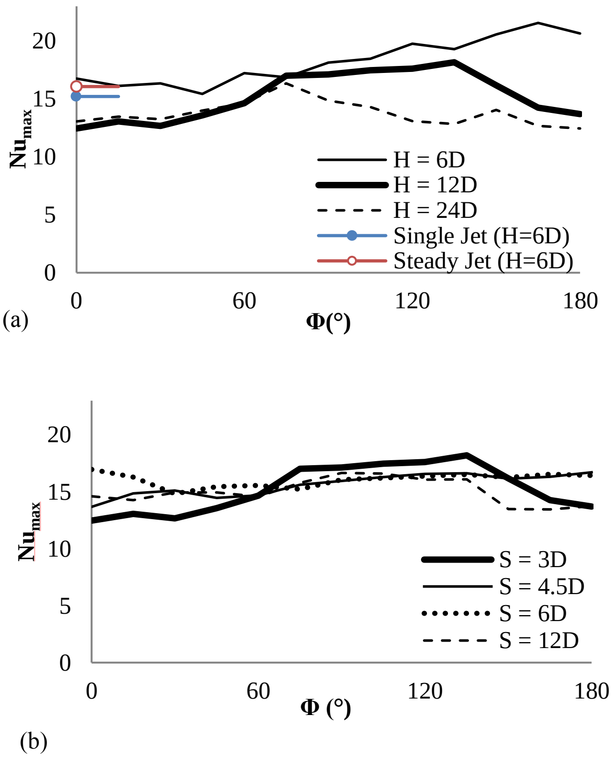

Figure 7 - Local maximum Nusselt number Nu_{max} as a function of phase difference for *Re* = 300, L_0/D = 29 (a) *S/D* = 3, *H/D* = 6, 12, 24, for a single synthetic jet and a steady jet [15] at *H/D* = 6; and (b) *H/D* = 12, *S/D* = 3, 4.5, 6 and 12

Another effect present at the larger *S/D* values, discussed in Section 3.1.2, is the effect of the inner vortices of each vortex pair becoming ‘trapped’ between their opposite jet. This is likely to reduce the intensity of the mixing of heated and ambient fluid since the inner vortices fail to migrate across the impingement surface.

Figure 7b shows an optimum orifice-to-orifice spacing of $S = 3D$ for the range of values tested. There is also little or no enhancement in Nu_{max} with phase difference as the distance between the orifices is increased. As explained in Section 3.1.2, larger values of *S/D* resulted in less attraction between opposite jets. As a result, the stagnation heat transfer rate from the train of vortex pairs is not as large.

In general, there is little or no variation with phase difference of the spatial-averaged Nusselt number Nu_{avg}.

3.2.3 Discussion of optimum performance

The contour maps in Figure 8 summarize the heat transfer results in terms of local maximum and spatial average Nusselt number for different parameter settings. The largest *H/D* value of 24 displays a Nu_{avg} value 19% and 12% higher than that of $H = 6D$ and $H = 12D$, respectively, when operated at optimum phase difference. The lowest *H/D* value of 6 displays a Nu_{max} value 24% and 16% higher than that of $H = 24D$ and $H = 12D$, respectively, when operated at optimum phase difference. Therefore, in highly localized (hotspot) cooling applications, a value of $H/D = 6$ operated within a phase difference region of $150° < \Phi < 180°$ gives the best cooling performance This region of optimum stagnation heat transfer can be seen in the contour plot in Figure 8a.

Figure 8b shows that the largest value of $H/D = 24$ operated within a phase difference region of $60° < \Phi < 120°$ gives the highest average Nusselt number, and therefore the best average cooling performance.

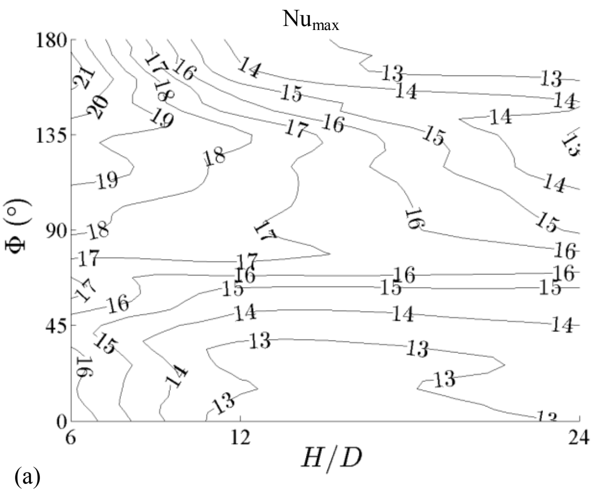

(a)

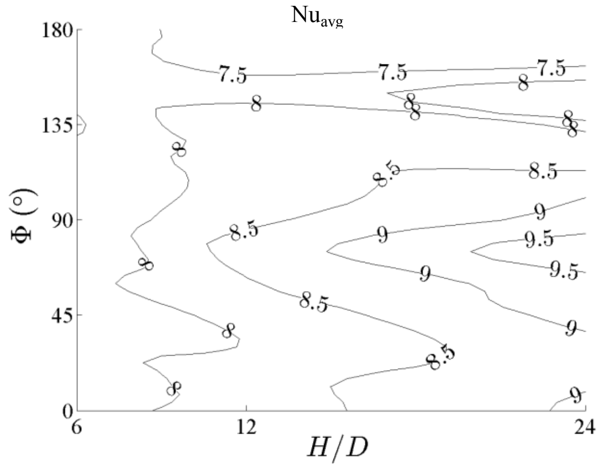

(b)

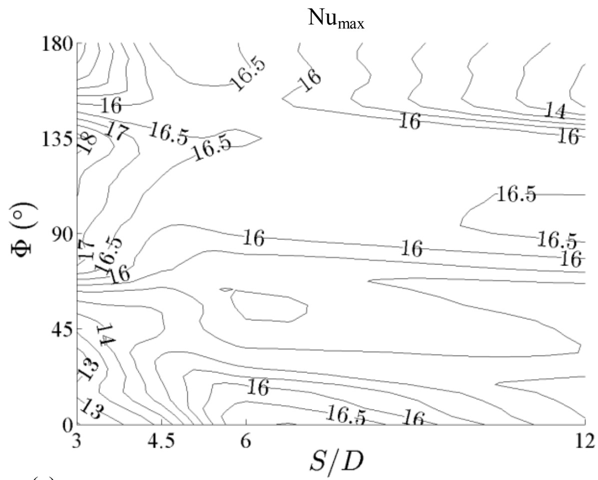

(c)

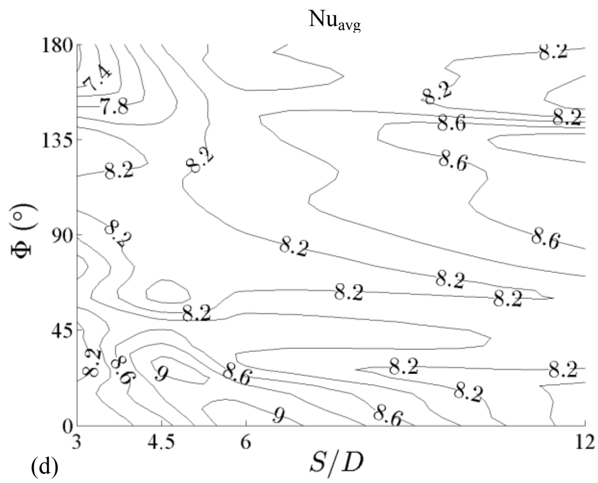

(d)

Figure 8 – Contour plots of Nu_{max} and Nu_{avg} versus Φ, (a,b) *H/D* and (c,d) *S/D*

For the intermediate *H/D* value of 12, when operated at an optimum phase difference, the smallest orifice separation of $S = 3D$ gives a Nu_{max} value 9% greater than each of the other settings ($S = 4.5D$, $6D$ and $12D$) which appear to be enhanced very little by phase difference (as shown in Figure 7b). Figure 8c demonstrates an optimum phase difference region of $75° < \Phi < 135°$ for the smallest orifice separation $S = 3D$. Thus it can be concluded that the smallest value of $S = 3D$ when operated within a phase difference region of $75° < \Phi < 135°$ gives the best cooling performance. In terms of the Nu_{avg} values, there is no clear optimum *S/D* setting. This is further illustrated in Figure 8d where the Nu_{avg} values range by very little across all values of Φ and *S/D*.

4. CONCLUSIONS

This research has investigated the convective heat transfer performance of two impinging synthetic jets operated side by side. The effect of the orifice-to-impingement distance *H* and orifice-to-orifice distance *S* on the convective heat transfer performance were explored as a function of varying phase difference Φ between the jets.

This performance has been quantified in terms of the local maximum and spatial average heat transfer coefficient and Nusselt number across an impingement foil, measured using a thermal imaging camera. These measurements were taken for a jet pair operating at a Reynolds number of $Re = 300$ and $L_0 = 29D$. Local velocity in the flow field of the jet has been measured using PIV measurements. The velocity measurements were also carried out for a stroke length of $L_0 = 29D$ and a Reynolds number of $Re \cong 265$.

The results have shown that increasing the jet-orifice-to-impingement distance from $H = 6D$ to $H = 24D$ produces a wider jet with higher average heat transfer. An enhancement in local maximum heat transfer with phase difference between the jets was exhibited for all values of *H/D* and this effect was particularly prominent for the lowest value of $H = 6D$. PIV measurements suggest that this enhancement is due to attraction of adjacent jets to form a train of vortex pairs impinging on the foil centre. PIV measurements also suggest possible critical values of H/Φ and S/Φ at which the inner vortices of the jet pair are subjected to a destructive interference resulting in a reduced convective heat transfer rate.

For the range of values tested, this study has revealed optimum geometric settings of $H = 24D$ and $S = 3D$ operated within a phase difference region of $60° < \Phi < 120°$ which give the best cooling performance.

ACKNOWLEDGEMENTS

Eoin Fanning is a research student under the Graduate Research Education Programme (GREP) in Engineering, which is funded by the Irish Government under the National Development Plan 2007-2013 with assistance of the European Regional Development Fund. Dr. Tim Persoons is a Marie Curie research fellow of the Irish Research Council for Science, Engineering and Technology (IRCSET).

REFERENCES

[1] Pavlova A and Amitay M 2006 Electronic Cooling Using Synthetic Jet Impingement *Journal of Heat Transfer* **128** 897 – 907

[2] Campbell Jr. S J, Black W Z, Glezer A and Hartley G J 1998 Thermal management of a laptop computer with synthetic air microjets *1998 Intersociety Conference on Thermal Phenomena* (IEEE) pp 43–50

[3] Mahalingam R, Williams R, Jones L and Heffington S 2007 Synthetic Jets for Forced Air Cooling of Electronics *Electronics Cooling* **13**

[4] Zhang J and Tan X 2007 Experimental study on flow and heat transfer characteristics of synthetic jet driven by piezoelectric actuator *Science in China Series E: Technological Sciences* **50** 221–9

[5] Silva L A and Ortega A 2010 Convective heat transfer due to an impinging synthetic jet: A numerical investigation of a canonical geometry *Thermal and Thermomechanical Phenomena in Electronic Systems (ITherm), 2010 12th IEEE Intersociety Conference on* (Las Vegas, NV, USA: IEEE) pp 1 – 8

[6] Shuster J M and Smith D R 2007 Experimental study of the formation and scaling of a round synthetic jet *Physics of Fluids* **19** 045109: 1–22

[7] Valiorgue P, Persoons T and McGuinn A 2009 Heat transfer mechanisms in an impinging synthetic jet for a small jet-to-surface spacing *Experimental and Thermal Fluid Science* **33** 597 – 603

[8] Persoons T, McGuinn A and Murray D B 2011 A general correlation for the stagnation point Nusselt number of an axisymmetric impinging synthetic jet *International Journal of Heat and Mass Transfer* **54** 3900–8

[9] Persoons T, O' Donovan T S and Murray D B 2009 Heat transfer in adjacent interacting impinging synthetic jets *ASME Summer Heat Transfer Conference* (San Francisco, CA, USA: ASME) pp 955–62

[10] Smith B L and Glezer A 2005 Vectoring of adjacent synthetic jets *AIAA journal* **43** 2117–24

[11] Luo Z-B and Xia Z-X 2008 PIV Measurements and Mechanisms of Adjacent Synthetic Jets Interactions *Chinese Physics Letters* **25** 612–5

[12] Persoons T and O'Donovan T S 2007 A pressure-based estimate of synthetic jet velocity *Physics of Fluids* **19** 128104

[13] Fanning E, Persoons T and Murray D B 2012 Heat transfer characteristics of a pair of impinging synthetic jets: Effect of orifice spacing and impingement distance *Journal of Physics: Conference Series* **395** 012025